Nanoscale Advances

PAPER

View Article Online
View Journal | View Issue

Cite this: *Nanoscale Adv.*, 2023, **5**, 6135

KHA model comprising MoS_4 and $CoFe_2O_3$ in engine oil invoking non-similar Darcy–Forchheimer flow with entropy and Cattaneo–Christov heat flux†

Sohail A. Khan, *[a] T. Hayat[a] and A. Alsaedi [b]

Objective: Nanoliquid flows are widely utilized in industrial, petroleum, engineering, and pharmaceutical applications including electric cooling, drug delivery, nuclear reactor cooling, solar collectors, heat exchangers, magnetohydrodynamic power generators, aerospace, porous media, thermal storage systems, and many others. Darcy–Forchheimer magnetized hybrid nanoliquid subjected to a stretchable cylinder was addressed, and the Cattaneo–Christov heat flux analysis was considered. Herein, disulfido (dithioxo) molybdenum (MoS_4) and cobalt ferrite ($CoFe_2O_4$) were considered as nanoparticles, and engine oil as a conventional liquid. The thermal relationship of heat generation and radiation was discussed, and the influence of the entropy rate was addressed. *Methodology*: Governing expressions were transformed into dimensionless forms. Simulation by the ND-solve technique was implemented. *Conclusions*: Features for the entropy rate, liquid flow, and temperature against emerging variables for nanoliquid (MoS_4/engine oil) and hybrid nanoliquid (MoS_4 + $CoFe_2O_4$/engine oil) were explored. The numerical results of the coefficient of skin friction and thermal transport rate for nanoliquid (MoS_4/engine oil) and hybrid nanoliquid (MoS_4 + $CoFe_2O_4$/engine oil) were examined. Reduction in velocity clearly occurred through a magnetic field, whereas the reverse impact held for the entropy rate. The thermal field and entropy rate against the curvature parameter were enhanced. A decrease in liquid flow occurred for higher porosity variables. An enhancement in the entropy rate was witnessed for radiation and porosity parameters. Higher radiation and thermal relaxation time variables resulted in enhancement of the thermal transport rate.

Received 21st June 2023
Accepted 11th September 2023

DOI: 10.1039/d3na00441d

rsc.li/nanoscale-advances

1. Introduction

Considerable research has been conducted on nanomaterials due to their significance in pharmaceutical, industrial, chemical, and engineering activities. Nanomaterial is basically created by the insertion of small-size (1–100 nm) particles in conventional liquid, which results in thermal conductivity enhancement. Nanomaterials play a key role in heat-related equipment, cooling and heating systems, radiators, nuclear reactors, fuel chambers, space technology, and caloric control. The initial investigations into nanofluids were conducted by Choi[1] and Eastman *et al.*[2] The distributed ultrafine particles efficiently strengthen the viscosity and thermal conductivity of nanomaterial and enhance its competence in energy exchange.[3,4] Thermal conductivity and viscosity may vary with the temperature of the nanofluid mixture, nanoparticle size, and volume fraction.

The thermal conductivity of metallic nanoparticles is higher than that of conventional materials, such as water and bioparticles with a lower density and thermal conductivity than that of traditional heat transfer fluids (HTFs). Sivasankaran *et al.*[5] addressed magnetohydrodynamic hybrid nanoliquid flow between stretchable parallel plates. Heat transport in the electromagnetohydrodynamic flow of Casson nanoliquid considering the heat source/sink was explored by Hussain *et al.*[6] Mixed convective flow of hybrid nanomaterial was explored by Patil and Shankar.[7] Çiçek *et al.*[8] explored the convective flow of hybrid nanofluid considering particle deposition inside a square cavity. There have been numerous investigations that have been conducted to explore nanofluid flow.[9–13]

A hybrid nanoliquid is the combination of two or more small size metallic nanoparticles with different chemical characteristics in conventional materials. Hybrid nanomaterials are useful to augment the advantages of nanoliquid such as heat transport transmission and enhancement processes. Because hybrid nanomaterials are advantageous for thermal conductivity enhancement, they are widely used in nuclear reactor

[a]*Department of Mathematics, Quaid-I-Azam University, P. O. Box 45320, Islamabad 44000, Pakistan. E-mail: sohailahmadkhan93@gmail.com*

[b]*Nonlinear Analysis and Applied Mathematics (NAAM) Research Group, Faculty of Science, King Abdulaziz University, P. O. Box 80207, Jeddah 21589, Saudi Arabia*

† KHA stands for Khan, Hayat and Alsaedi.

cooling processes, biomedical applications, solar energy, the automotive industry, automobile generators, space technology, and heat exchangers.

Thermal enhancement of convectional material by insertion of single particles and hybrid nanoparticles was given in Jana *et al.*[14] Bhatti *et al.*[15] discussed the magnetohydrodynamic flow of hybrid nanomaterial by a circular non-Darcy surface. Wahid *et al.*[16] analyzed heat transfer in hybrid nanomaterial subject to a Riga plate. Slip impacts in the convection stagnation point flow of hybrid nanoliquid were reported by Zangooee *et al.*[17] Khan *et al.*[18] explored entropy in a radiating flow of hybrid nanoliquid through the Darcy–Forchheimer relation. Zainal *et al.*[19] deliberated the influence of Arrhenius kinetics in hybrid nanomaterial flow by a shrinking and stretching surface with radiation. It should be noted that there have been few attempts to study hybrid nanoliquid flow.[20–30]

Entropy generation is the measurement of energy wastage during any thermal process. Entropy always increases in an irreversible process, and therefore, entropy generation is a positive quantity. Entropy generation is also a non-conserved property. There is no existence of conservation of entropy. Therefore, the entropy of the universe is continuously increasing. Joule heating, fluid flow friction between solid surfaces, molecular vibration, liquid viscosity, and diffusion are sources that produce entropy generation. In fact, Bejan discovered entropy optimization for convective flow with thermal convection.[31,32] Entropy for the radiative magnetized flow of a hybrid nanoliquid due to a stretchable rotating disk is presented in Khan *et al.*[33] Kumawat *et al.*[34] analyzed magnetized entropy-optimized flow with variable viscosity. Nonlinear radiation in hybridized nanoliquid flow with a convectively heated surface was explored by Ashwinkumar *et al.*[35] Rajkumar *et al.*[36] examined Cattaneo–Christov flux in the radiative flow of micropolar nanofluid with entropy optimization. Similar studies on entropy have been conducted.[37–42]

The main theme here is to communicate the Cattaneo–Christov heat flux for the magnetohydrodynamic flow of hybrid (MoS_4 + $CoFe_2O_4$/engine oil) nanoliquid towards a stretchable cylinder. The Darcy–Forchheimer relation is used for porous space. Disulfido (dithioxo) molybdenum (MoS_4) and cobalt ferrite ($CoFe_2O_4$) are considered as nanoparticles, and engine oil as a conventional fluid. Cattaneo–Christov heat flux was deliberated, and radiation and heat generation were considered. Entropy optimization was also considered. Related equations were converted into dimensionless versions. The ND-solve technique was implemented for solution of nonlinear non-dimensional systems. Fluid flow, entropy rate, and temperature *via* the involved variables for nanoliquid (MoS_4/engine oil) and hybrid nanoliquid (MoS_4 + $CoFe_2O_4$/engine oil) were graphically analyzed. The numerical results illustrating the impacts of influential variables on physical quantities for nanoliquid (MoS_4/engine oil) and hybrid nanoliquid (MoS_4 + $CoFe_2O_4$/engine oil) are presented.

2. Formulation

The hydromagnetic flow of hybrid (MoS_4 + $CoFe_2O_4$/engine oil) nanomaterial by stretchable porous cylinder was examined. The Darcy–Forchheimer expression was used for porous space. Cattaneo–Christov heat flux was carried out. Disulfido

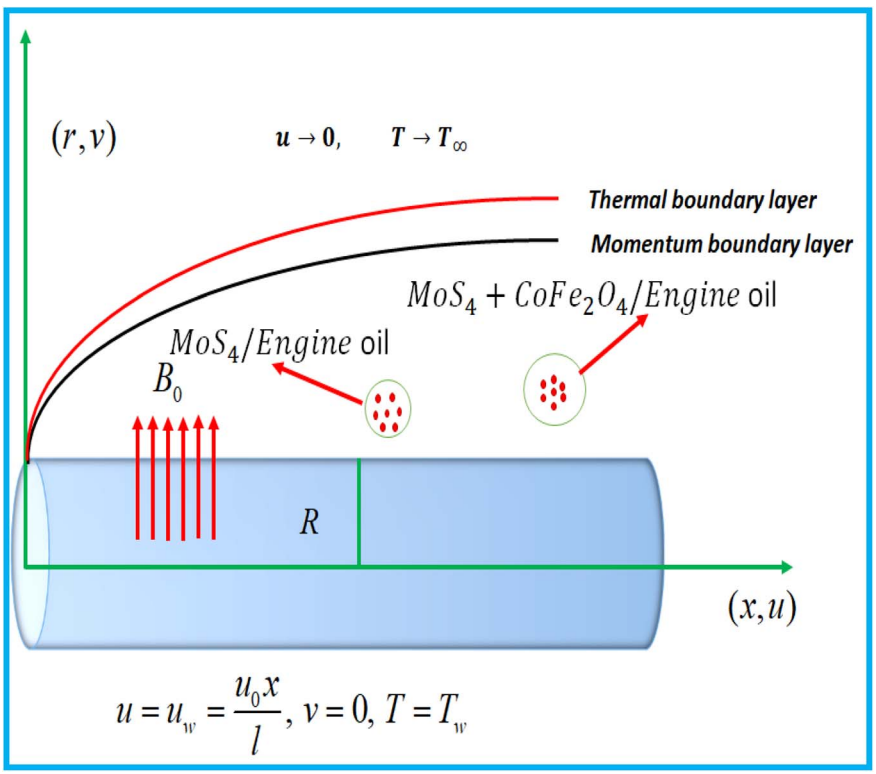

Fig. 1 Physical model.

Table 1 Values of nanoparticles and base liquid[50–53]

Physical property	ρ_f (kg m^{-3})	$(C_p)_f$ (J kg^{-1} K^{-1})	σ_f (S m^{-1})	k_f (W m^{-1} K^{-1})
Engine oil	884	1910	10^{-11} to 2×10^{-9}	0.1410
MoS_4	5060	397.21	2.09×10^4	904.4
$CoFe_2O_4$	4907	700	5.51×10^9	3.7

(dithioxo) molybdenum (MoS_4) and cobalt ferrite ($CoFe_2O_4$) were considered as nanoparticles, and engine oil as a conventional material. Radiation and heat generation were present in the energy equation, and entropy modeling was carried out. A constant magnetic field (B_0) perpendicular to the liquid flow was applied. The radius of a cylinder was considered as (R), and stretching velocity $\left(u = u_w = \frac{u_0 x}{l}\right)$ (l shows characteristics length). The flow configuration is sketched in Fig. 1.

Under these considerations, the related expressions are:[43–48]

$$\frac{\partial(rv)}{\partial r} + \frac{\partial(ru)}{\partial x} = 0, \tag{1}$$

$$u\frac{\partial u}{\partial x} + v\frac{\partial u}{\partial r} = \frac{\mu_{hnf}}{\rho_{hnf}}\left(\frac{\partial^2 u}{\partial r^2} + \frac{1}{r}\frac{\partial u}{\partial r}\right) - \frac{\sigma_{hnf}B_0{}^2}{\rho_{hnf}}u - \frac{\mu_{hnf}}{\rho_{hnf}}\frac{1}{k_p}u - Fu^2, \tag{2}$$

$$\left.\begin{aligned} &u\frac{\partial T}{\partial x} + v\frac{\partial T}{\partial r} - \frac{1}{(\rho c_p)_{hnf}}\frac{16\sigma^* T_\infty{}^3}{3k^*}\left(\frac{1}{r}\frac{\partial T}{\partial r} + \frac{\partial^2 T}{\partial r^2}\right) - \frac{Q_0}{(\rho c_p)_{hnf}}(T - T_\infty) \\ &+ \delta_E\left(u^2\frac{\partial^2 T}{\partial x^2} + u\frac{\partial u}{\partial x}\frac{\partial T}{\partial x} + u\frac{\partial v}{\partial x}\frac{\partial T}{\partial r} + 2uv\frac{\partial^2 T}{\partial x\partial r} + v\frac{\partial u}{\partial r}\frac{\partial T}{\partial x} + v\frac{\partial v}{\partial r}\frac{\partial T}{\partial r} + v^2\frac{\partial^2 T}{\partial r^2}\right) \\ &-\delta_E\frac{1}{(\rho c_p)_{hnf}}\frac{16\sigma^* T_\infty{}^3}{3k^*}\left(\frac{u}{r}\frac{\partial^2 T}{\partial x\partial r} + u\frac{\partial^3 T}{\partial x\partial r^2} - \frac{v}{r^2}\frac{\partial T}{\partial r} + \frac{v}{r}\frac{\partial^2 T}{\partial r^2} + v\frac{\partial^3 T}{\partial r^3}\right) \\ &-\delta_E\frac{Q_0}{(\rho c_p)_{hnf}}\left(u\frac{\partial T}{\partial x} + v\frac{\partial T}{\partial r}\right) = \frac{k_{hnf}}{(\rho c_p)_{hnf}}\left(\frac{1}{r}\frac{\partial T}{\partial r} + \frac{\partial^2 T}{\partial r^2}\right) \end{aligned}\right\}, \tag{3}$$

with

$$\left.\begin{aligned} &u = u_w(x) = \frac{u_0 x}{l}, v = 0, T = T_w, \text{at } r = R \\ &u \to 0, T \to T_\infty, \text{as } r \to \infty \end{aligned}\right\}, \tag{4}$$

in which (u,v) represent velocity components, μ_{hnf} the dynamic viscosity, σ_{hnf} the electrical conductivity, (x,r) the cylindrical coordinates, $F\left(= \frac{C_b}{\sqrt{k_p}}\right)$ the inertia coefficient, ρ_{hnf} the density, k_p the porous space permeability, ν_{hnf} the kinematic viscosity, C_b the drag force coefficient, T the temperature, $(C_p)_{hnf}$ specific heat, $Q_0 > 0$ the heat generation coefficient, σ^* Stefan Boltzmann constant, $\alpha_f\left(= \frac{k_f}{(\rho c_p)_f}\right)$ thermal diffusivity, k^* mean absorption coefficient, k_{hnf} the thermal conductivity, δ_E the thermal relaxation time, T_w the wall temperature, u_0 the reference velocity, and T_∞ the ambient temperature.

2.1. Thermophysical characteristics

The thermophysical characteristics were determined by Hamilton–Crosser relations for the nanomaterial and hybrid nanomaterial (Table 1).[49]

2.1.1. Viscosity

$$\mu_{nf} = \frac{\mu_f}{(1-\phi_1)^{2.5}} \text{ for nanoliquid,} \tag{5}$$

$$\mu_{hnf} = \frac{\mu_f}{(1-\phi_1)^{2.5}(1-\phi_2)^{2.5}} \text{ for hybrid nanoliquid,} \tag{6}$$

2.1.2. Density

$$\rho_{nf} = (1-\phi_1)\rho_f + \phi_1\rho_{s1} \text{ for nanoliquid,} \tag{7}$$

$$\rho_{hnf} = (1-\phi_2)[(1-\phi_1)\rho_f + \phi_1\rho_{s1}] + \phi_2\rho_{s2} \text{ for hybrid nanoliquid.} \tag{8}$$

2.1.3. Electrical conductivity

$$\frac{\sigma_{nf}}{\sigma_f} = \frac{\sigma_{s1} + (n-1)\sigma_f - (n-1)\phi_1(\sigma_f - \sigma_{s1})}{\sigma_{s1} + (n-1)\sigma_f + \phi_1(\sigma_f - \sigma_{s1})} \text{ for nanoliquids.} \tag{9}$$

$$\frac{\sigma_{hnf}}{\sigma_{nf}} = \frac{\sigma_{s2} + (n-1)\sigma_{nf} - (n-1)\phi_2(\sigma_{nf} - \sigma_{s2})}{\sigma_{s2} + (n-1)\sigma_{nf} + \phi_2(\sigma_{nf} - \sigma_{s2})} \text{ for hybrid nanoliquid.} \tag{10}$$

2.1.4. Specific heat capacity

$$(\rho c_p)_{nf} = (1-\phi_1)(\rho c_p)_f + \phi_1(\rho c_p)_{s1} \text{ for nanoliquid,} \tag{11}$$

$$(\rho c_p)_{hnf} = (1-\phi_2)[(1-\phi_1)(\rho c_p)_f + \phi_1(\rho c_p)_{s1}] + \phi_2(\rho c_p)_{s2} \text{ for hybrid nanoliquid.} \tag{12}$$

2.1.5. Thermal conductivity

$$\frac{k_{nf}}{k_f} = \frac{k_{s1} + (n-1)k_f - (n-1)\phi_1(k_f - k_{s1})}{k_{s1} + (n-1)k_f + \phi_1(k_f - k_{s1})} \text{for nanoliquid,} \quad (13)$$

$$\frac{k_{hnf}}{k_{nf}} = \frac{k_{s2} + (n-1)k_{nf} - (n-1)\phi_2(k_{nf} - k_{s2})}{k_{s2} + (n-1)k_{nf} + \phi_2(k_{nf} - k_{s2})} \text{for hybrid nanoliquid.} \quad (14)$$

Considering transformations

$$\left.\begin{aligned} &\xi = \frac{x}{l}, \eta = \sqrt{\frac{u_0}{l\nu_f}}\left(\frac{r^2 - R^2}{2R}\right), u = u_0\xi\frac{\partial f}{\partial \eta}(\xi,\eta), \\ &v = -\frac{1}{r}\sqrt{\frac{\nu_f u_0}{l}}Rf(\xi,\eta) - \frac{1}{r}\sqrt{\frac{\nu_f u_0}{l}}\xi R\frac{\partial f}{\partial \xi}(\xi,\eta), \\ &\theta(\xi,\eta) = \frac{T - T_\infty}{T_w - T_\infty}, u_w = \frac{u_0 x}{l}, \end{aligned}\right\} \quad (15)$$

$$\left.\begin{aligned} &(1+2\alpha\eta)\frac{\partial^3 f}{\partial \eta^3} + 2\alpha\frac{\partial^2 f}{\partial \eta^2} - A_1A_2\left(\frac{\partial f}{\partial \eta}\right)^2 + A_1A_2 f\frac{\partial^2 f}{\partial \eta^2} - A_1A_2\xi\frac{\partial^2 f}{\partial \xi\partial \eta}\frac{\partial f}{\partial \eta} + A_1A_2\xi\frac{\partial f}{\partial \xi}\frac{\partial^2 f}{\partial \eta^2} \\ &-\lambda\frac{\partial f}{\partial \eta} - A_1A_2\mathrm{Fr}\xi\left(\frac{\partial f}{\partial \eta}\right)^2 - A_1\frac{\sigma_{hnf}}{\sigma_f}M\frac{\partial f}{\partial \eta} = 0 \end{aligned}\right\}, \quad (16)$$

$$\left.\begin{aligned} &\left(\frac{k_{hnf}}{k_f} + \mathrm{Rd}\right)\left((1+2\alpha\eta)\frac{\partial^2\theta}{\partial \eta^2} + 2\alpha\frac{\partial \theta}{\partial \eta}\right) - A_3\mathrm{Pr}\xi\frac{\partial f}{\partial \eta}\frac{\partial \theta}{\partial \xi} + A_3\mathrm{Pr}f(\xi,\eta)\frac{\partial \theta}{\partial \eta} + A_3\mathrm{Pr}\xi\frac{\partial f}{\partial \xi}\frac{\partial \theta}{\partial \eta} + \mathrm{Pr}Q\theta \\ &-A_3\mathrm{Pr}\beta_t A^* + \beta_t\mathrm{Rd}A^{**} + \mathrm{Pr}\beta_t Q\left(\xi\frac{\partial \theta}{\partial \xi}\frac{\partial f}{\partial \eta} - f\frac{\partial \theta}{\partial \eta} - \xi\frac{\partial \theta}{\partial \eta}\frac{\partial f}{\partial \xi}\right) = 0 \end{aligned}\right\}, \quad (17)$$

with

$$A^* = \left(\begin{aligned} &-2\xi\frac{\partial f}{\partial \xi}\frac{\partial f}{\partial \eta}\frac{\partial \theta}{\partial \eta} + \xi^2\left(\frac{\partial f}{\partial \eta}\right)^2\frac{\partial^2\theta}{\partial \xi^2} + \xi^2\frac{\partial f}{\partial \eta}\frac{\partial^2 f}{\partial \xi\partial \eta}\frac{\partial \theta}{\partial \xi} + \xi\left(\frac{\partial f}{\partial \eta}\right)^2\frac{\partial \theta}{\partial \xi} - \xi^2\frac{\partial f}{\partial \eta}\frac{\partial \theta}{\partial \eta}\frac{\partial^2 f}{\partial \xi^2} \\ &-2f\xi\frac{\partial f}{\partial \eta}\frac{\partial^2\theta}{\partial \xi\partial \eta} - 2\xi^2\frac{\partial f}{\partial \eta}\frac{\partial f}{\partial \xi}\frac{\partial^2\theta}{\partial \xi\partial \eta} - f\xi\frac{\partial \theta}{\partial \xi}\frac{\partial^2 f}{\partial \eta^2} - \xi^2\frac{\partial f}{\partial \xi}\frac{\partial \theta}{\partial \xi}\frac{\partial^2 f}{\partial \eta^2} \\ &-\left(\frac{\alpha}{(1+2\alpha\eta)}\right)\xi f\frac{\partial f}{\partial \xi}\frac{\partial \theta}{\partial \eta} + f\xi\frac{\partial \theta}{\partial \eta}\frac{\partial^2 f}{\partial \xi\partial \eta} - \left(\frac{\alpha}{(1+2\alpha\eta)}\right)\xi^2\frac{\partial \theta}{\partial \eta}\left(\frac{\partial f}{\partial \xi}\right)^2 \\ &-\left(\frac{\alpha}{(1+2\alpha\eta)}\right)f\xi\frac{\partial f}{\partial \xi}\frac{\partial \theta}{\partial \eta} + \xi^2\frac{\partial f}{\partial \xi}\frac{\partial \theta}{\partial \eta}\frac{\partial^2 f}{\partial \eta\partial \xi} + f^2\frac{\partial^2\theta}{\partial \eta^2} + \xi\frac{\partial f}{\partial \eta}\frac{\partial \theta}{\partial \eta}\frac{\partial f}{\partial \xi} + f\frac{\partial f}{\partial \eta}\frac{\partial \theta}{\partial \eta} \\ &+2\left(\frac{\alpha}{(1+2\alpha\eta)}\right)f\xi\frac{\partial f}{\partial \xi}\frac{\partial \theta}{\partial \eta} + 2f\xi\frac{\partial f}{\partial \xi}\frac{\partial^2\theta}{\partial \eta^2} + \xi^2\left(\frac{\partial f}{\partial \xi}\right)^2\frac{\partial^2\theta}{\partial \eta^2} \\ &+\left(\frac{\alpha}{(1+2\alpha\eta)}\right)\xi^2\left(\frac{\partial f}{\partial \xi}\right)^2\frac{\partial \theta}{\partial \eta} \end{aligned}\right), \quad (19)$$

we have

$$\left.\begin{aligned} &\frac{\partial f}{\partial \eta}(\xi,0) = 1, f(\xi,0) = -\xi\frac{\partial f}{\partial \xi}(\xi,0), \theta(\xi,0) = 1 \\ &\frac{\partial f}{\partial \eta}(\xi,\infty) = 0, \theta(\xi,\infty) = 0 \end{aligned}\right\}. \quad (18)$$

In the above expressions, $\alpha\left(=\sqrt{\frac{\nu_f l}{u_0 R^2}}\right)$ indicates the curvature variable, $M\left(=\frac{\sigma_f {B_0}^2 l}{U_0\rho_f}\right)$ the magnetic parameter, $\lambda\left(=\frac{\nu_f l}{u_0 k_p}\right)$ the porosity variable, $\mathrm{Pr}\left(=\frac{\nu_f}{\alpha_f}\right)$ the Prandtl

number, $\mathrm{Fr}\left(=\frac{C_b}{\sqrt{k_p}}l\right)$ the Forchheimer number, $\mathrm{Rd}\left(=\frac{16\sigma^* {T_\infty}^3}{3k^* k_f}\right)$ the radiation parameter, $\beta_t\left(\frac{\delta_E l}{u_0}\right)$ the thermal relaxation time variable, and $Q\left(=\frac{Q_0 l}{u_o(\rho c_p)_f}\right)$. A^*, A^{**}, A_1, A_2 and A_3 are

$$A^{**} = \begin{pmatrix} 2\xi\alpha\frac{\partial f}{\partial\eta}\frac{\partial^2\theta}{\partial\xi\partial\eta} + \xi(1+2\alpha\eta)\frac{\partial f}{\partial\eta}\frac{\partial^3\theta}{\partial\xi\partial\eta^2} - 4\alpha f\frac{\partial^2\theta}{\partial\eta^2} - (1+2\alpha\eta)f\frac{\partial^3\theta}{\partial\eta^3} \\ -4\alpha\xi\frac{\partial f}{\partial\xi}\frac{\partial^2\theta}{\partial\eta^2} - (1+2\alpha\eta)\xi\frac{\partial f}{\partial\xi}\frac{\partial^3 f}{\partial\eta^3} \end{pmatrix} \tag{20}$$

$$A_1 = (1-\phi_1)^{2.5}(1-\phi_2)^{2.5} \tag{21}$$

$$A_2 = (1-\phi_2)\left[(1-\phi_1) + \phi_1\frac{\rho_{s1}}{\rho_f}\right] + \phi_2\frac{\rho_{s2}}{\rho_f} \tag{22}$$

$$A_3 = (1-\phi_2)\left[(1-\phi_1) + \phi_1\frac{(\rho c_p)_{s1}}{(\rho c_p)_f}\right] + \phi_2\frac{(\rho c_p)_{s2}}{(\rho c_p)_f} \tag{23}$$

3. Quantities under interest

Skin friction coefficient $\left(\frac{1}{2}C_{fx}{\mathrm{Re}_x}^{1/2}\right)$ and Nusselt number $(\mathrm{Nu}_x\mathrm{Re}_x^{-1/2})$ are

$$\left.\begin{aligned} C_{fx} &= \frac{2\tau_w}{\rho_f {u_w}^2} \\ \mathrm{Nu}_x &= \frac{x q_w}{k_f(T_w - T_\infty)} \end{aligned}\right\}. \tag{24}$$

Shear stress (τ_w) and heat flux (q_w) satisfy

$$\left.\begin{aligned} \tau_w &= \mu_{hnf}\left(\frac{\partial u}{\partial r}\right)\Big|_{r=R} \\ q_w &= -\left(k_{hnf} + \frac{16\sigma^* {T_\infty}^3}{3k^*}\right)\left(\frac{\partial T}{\partial r}\right)\Big|_{r=R} \end{aligned}\right\} \tag{25}$$

One may write eqn (27) and (28) as

$$\left.\begin{aligned} \frac{1}{2}C_{fx}{\mathrm{Re}_x}^{1/2} &= \frac{1}{A_1}f''(0) \\ \mathrm{Nu}_x\mathrm{Re}_x^{-1/2} &= -\left(\frac{k_{hnf}}{k_f} + Rd\right)\theta'(0) \end{aligned}\right\}, \tag{26}$$

where $\mathrm{Re}_x\left(=\frac{u_w x}{\nu_f}\right)$ shows the local Reynolds number.

4. Expression for entropy

Mathematically, entropy is expressed as

$$\left.\begin{aligned} E_G = \frac{k_f}{{T_\infty}^2}\left(\frac{k_{hnf}}{k_f} + \frac{16\sigma^* {T_\infty}^3}{3k^* k_f}\right)\left(\frac{\partial T}{\partial r}\right)^2 + \frac{\mu_{hnf}}{T_\infty}\left(\frac{\partial u}{\partial r}\right)^2 \\ + \frac{\sigma_{hnf}{B_0}^2}{T_\infty}u^2 + \frac{\mu_{hnf}}{k_p T_\infty}u^2 \end{aligned}\right\}. \tag{27}$$

The above expression can be reduced as

$$\left.\begin{aligned} N_G(\eta) = \alpha_1\left(\frac{k_{hnf}}{k_f} + \mathrm{Rd}\right)(1+2\alpha\eta)\left(\frac{\partial\theta}{\partial\eta}\right)^2 + \frac{\mathrm{Br}}{A_1}\xi^2(1+2\alpha\eta)\left(\frac{\partial^2 f}{\partial\eta^2}\right)^2 + \frac{\lambda\mathrm{Br}}{A_1}\xi^2\left(\frac{\partial f}{\partial\eta}\right)^2 \\ + \frac{\sigma_{hnf}}{\sigma_f}M\mathrm{Br}\xi^2\left(\frac{\partial f}{\partial\eta}\right)^2 \end{aligned}\right\}, \tag{28}$$

where $N_G\left(=\frac{E_G\nu_f l T_\infty}{k_f u_0(T_w - T_\infty)}\right)$ characterizes the entropy rate, $\alpha_1\left(=\frac{(T_w - T_\infty)}{T_\infty}\right)$ the temperature difference variable, and $\mathrm{Br}\left(=\frac{\mu_f {u_0}^2}{k_f(T_w - T_\infty)}\right)$ the Brinkman number.

5. Solution development

5.1. Local similar solution

To obtain a local similar solution, we suppose that $\frac{\partial(\cdot)}{\partial\xi} = 0$ and denote $\frac{\partial(\cdot)}{\partial\eta}$ by prime in eqn (16)–(18). We have

$$\left.\begin{aligned} (2\alpha\eta+1)f''' + 2\alpha f'' - A_1A_2f'^2 + A_1A_2ff'' - \lambda f' - A_1A_2\mathrm{Fr}\xi f'^2 \\ - \frac{\sigma_{hnf}}{\sigma_f}A_1Mf' = 0 \end{aligned}\right\}, \tag{29}$$

$$\left.\begin{aligned} \left(\frac{k_{hnf}}{k_f} + \mathrm{Rd}\right)\left(2\alpha\theta' + (2\alpha\eta+1)\theta''\right) + A_3\mathrm{Pr}f\theta' + \mathrm{Pr}Q\theta - \beta_t\mathrm{Pr}\left(f^2\theta'' + ff'\theta'\right) \\ - \beta_t\mathrm{Rd}\left((2\alpha\eta+1)f\theta''' + 4\alpha f\theta''\right) - \beta_t\mathrm{Pr}QF\theta' = 0 \end{aligned}\right\}, \tag{30}$$

$$\left.\begin{array}{c} f'(0)=1, f(0)=0, \theta(0)=1 \\ f'(\infty)=0, \theta(\infty)=0 \end{array}\right\}. \quad (31)$$

5.2. Local non-similar solution

To construct the local non-similar solution, we suppose that $\frac{\partial f}{\partial \xi}=p$, $\frac{\partial^2 f}{\partial \xi \partial \eta}=\frac{\partial p}{\partial \eta}$, $\frac{\partial^3 f}{\partial \xi \partial \eta^2}=\frac{\partial^2 p}{\partial \eta^2}$, $\frac{\partial^2 f}{\partial \xi^2}=\frac{\partial p}{\partial \xi}$, $\frac{\partial \theta}{\partial \xi}=q$, $\frac{\partial^2 \theta}{\partial \xi \partial \eta}=\frac{\partial q}{\partial \eta}$, $\frac{\partial^3 \theta}{\partial \xi \partial \eta^2}=\frac{\partial^2 q}{\partial \eta^2}$, $\frac{\partial^2 \theta}{\partial \xi^2}=\frac{\partial q}{\partial \xi}$ in eqn (16)–(18). One obtains

$$\left.\begin{array}{c} (2\alpha\eta+1)\frac{\partial^3 f}{\partial \eta^3}+2\alpha\frac{\partial^2 f}{\partial \eta^2}-A_1A_2\left(\frac{\partial f}{\partial \eta}\right)^2+A_1A_2 f\frac{\partial^2 f}{\partial \eta^2}-A_1A_2\xi\frac{\partial p}{\partial \eta}\frac{\partial f}{\partial \eta}+A_1A_2\xi P\frac{\partial^2 f}{\partial \eta^2} \\ -\lambda\frac{\partial f}{\partial \eta}-A_1A_2\mathrm{Fr}\left(\frac{\partial f}{\partial \eta}\right)^2-A_1\frac{\sigma_{\mathrm{hnf}}}{\sigma_{\mathrm{f}}}M\frac{\partial f}{\partial \eta}=0 \end{array}\right\}, \quad (32)$$

$$\left.\begin{array}{c} \left(\frac{k_{\mathrm{hnf}}}{k_{\mathrm{f}}}+\mathrm{Rd}\right)\left[(2\alpha\eta+1)\frac{\partial^2 \theta}{\partial \eta^2}+2\alpha\frac{\partial \theta}{\partial \eta}\right]-A_3\mathrm{Pr}\xi\frac{\partial f}{\partial \eta}q+A_3\mathrm{Pr}f\frac{\partial \theta}{\partial \eta}+A_3\mathrm{Pr}\xi p\frac{\partial \theta}{\partial \eta} \\ +\mathrm{Pr}Q\theta-A_3\mathrm{Pr}\beta_{\mathrm{t}}A_{11}+\beta_{\mathrm{t}}\mathrm{Rd}A_{22}+\mathrm{Pr}\beta_{\mathrm{t}}Q\left(\xi q\frac{\partial f}{\partial \eta}-f\frac{\partial \theta}{\partial \eta}-\xi p\frac{\partial \theta}{\partial \eta}\right)=0 \end{array}\right\}, \quad (33)$$

$$\left.\begin{array}{c} \frac{\partial f}{\partial \eta}(\xi,0)=1, f(\xi,0)=-\xi p(\xi,0), \theta(\xi,0)=1 \\ \frac{\partial f}{\partial \eta}(\xi,\infty)=0, \theta(\xi,\infty)=0 \end{array}\right\}. \quad (34)$$

In the above equations, A_{11} and A_{22} are defined as

$$A_{11}=\left[\begin{array}{c} -2\xi P\frac{\partial f}{\partial \eta}\frac{\partial \theta}{\partial \eta}+\xi^2\left(\frac{\partial f}{\partial \eta}\right)^2\frac{\partial q}{\partial \xi}+\xi^2 q\frac{\partial f}{\partial \eta}\frac{\partial p}{\partial \eta}+\xi q\left(\frac{\partial f}{\partial \eta}\right)^2-\xi^2\frac{\partial f}{\partial \eta}\frac{\partial \theta}{\partial \eta}\frac{\partial p}{\partial \xi} \\ -2\xi f\frac{\partial f}{\partial \eta}\frac{\partial q}{\partial \eta}-2\xi^2 p\frac{\partial f}{\partial \eta}\frac{\partial q}{\partial \eta}-\xi f q\frac{\partial^2 f}{\partial \eta^2}-\xi^2 p q\frac{\partial^2 f}{\partial \eta^2}-\left(\frac{\alpha}{(2\alpha\eta+1)}\right)\xi f p\frac{\partial \theta}{\partial \eta} \\ +\xi f\frac{\partial \theta}{\partial \eta}\frac{\partial p}{\partial \eta}-\left(\frac{\alpha}{(2\alpha\eta+1)}\right)\xi^2 p^2\frac{\partial \theta}{\partial \eta}-\left(\frac{\alpha}{(2\alpha\eta+1)}\right)\xi f p\frac{\partial \theta}{\partial \eta}+\xi^2 p\frac{\partial \theta}{\partial \eta}\frac{\partial p}{\partial \eta} \\ +f^2\frac{\partial^2 \theta}{\partial \eta^2}+\xi p\frac{\partial f}{\partial \eta}\frac{\partial \theta}{\partial \eta}+f\frac{\partial f}{\partial \eta}\frac{\partial \theta}{\partial \eta}+2\left(\frac{\alpha}{(2\alpha\eta+1)}\right)\xi f p\frac{\partial \theta}{\partial \eta}+2\xi f p\frac{\partial^2 \theta}{\partial \eta^2} \\ +\xi^2 p^2\frac{\partial^2 \theta}{\partial \eta^2}+\left(\frac{\alpha}{(2\alpha\eta+1)}\right)\xi^2 p^2\frac{\partial \theta}{\partial \eta} \end{array}\right], \quad (35)$$

$$A_{22}=\left[\begin{array}{c} 2\alpha\xi\frac{\partial f}{\partial \eta}\frac{\partial q}{\partial \eta}+\xi(2\alpha\eta+1)\frac{\partial f}{\partial \eta}\frac{\partial^2 q}{\partial \eta^2}-4\alpha f\frac{\partial^2 \theta}{\partial \eta^2}-(2\alpha\eta+1)f\frac{\partial^3 \theta}{\partial \eta^3} \\ -4\alpha\xi p\frac{\partial^2 \theta}{\partial \eta^2}-(2\alpha\eta+1)\xi p\frac{\partial^3 f}{\partial \eta^3} \end{array}\right] \quad (36)$$

We take the derivative of eqn (32)–(34) with respect to "ξ" and representing $\frac{\partial(\cdot)}{\partial \eta}$ by prime. Suppose that $\frac{\partial p}{\partial \xi}$, $\frac{\partial^2 p}{\partial \xi \partial \eta}$, $\frac{\partial^3 p}{\partial \xi \partial \eta^2}$, $\frac{\partial q}{\partial \xi}$, $\frac{\partial^2 q}{\partial \xi \partial \eta}$, $\frac{\partial^3 q}{\partial \xi \partial \eta^2}$, $\frac{\partial g}{\partial \xi}$, $\frac{\partial^2 g}{\partial \xi \partial \eta}$, $\frac{\partial^3 g}{\partial \xi \partial \eta^2}$ become zero. We obtain

$$\left.\begin{aligned}&(2\alpha\eta+1)p'''+2\alpha p''-2A_1A_2f'p'+A_1A_2pf''+A_1A_2fp''-A_1A_2p'f'-A_1A_2\xi p'^2\\&+A_1A_2pf''+A_1A_2\xi pp''-\lambda p'-A_1A_2\mathrm{Fr}f'^2-2A_1A_2\mathrm{Fr}\xi f'p'-A_1\frac{\sigma_{\mathrm{hnf}}}{\sigma_{\mathrm{f}}}MP'=0\end{aligned}\right\},\tag{37}$$

$$\left.\begin{aligned}&\left(\frac{k_{\mathrm{hnf}}}{k_{\mathrm{f}}}+\mathrm{Rd}\right)\left[(2\alpha\eta+1)q''+2\alpha q'\right]-A_3\mathrm{Pr}f'q-A_3\mathrm{Pr}\xi p'q+A_3\mathrm{Pr}p\theta'+A_3\mathrm{Pr}fq'\\&+A_3\mathrm{Pr}p\theta'+A_3\mathrm{Pr}\xi pq'+\mathrm{Pr}Qq-A_3\mathrm{Pr}\beta_{\mathrm{t}}A_{33}+\mathrm{Rd}\beta_{\mathrm{t}}A_{44}\\&+\mathrm{Pr}Q\beta_{\mathrm{t}}\left(qf'+\xi qp'-p\theta'-fq'-p\theta'-\xi pq'\right)=0,\end{aligned}\right\},\tag{38}$$

$$\left.\begin{aligned}p'(\xi,0)=0,p(\xi,0)=0,q(\xi,0)=0\\p'(\xi,\infty)=0,q(\xi,\infty)=0\end{aligned}\right\}.\tag{39}$$

In the above equation, A_{33} and A_{44} are expressed as

$$A_{33}=\begin{bmatrix}-7\xi Pf'q'+4\xi f'p'q+\xi^2p'^2q+f'^2q-2fp'q'-\xi fp'q'-\xi^2pp'q'-fqf''-3\xi pqf''+f^2q''\\-\xi fqp''-\xi^2pqp''+2fp'\theta'+2\xi pp'\theta'+4fp\theta''+ff'q'+4\xi p^2\theta''+2\xi fpq''+\xi^2p^2q''\end{bmatrix}\tag{40}$$

$$A_{44}=\begin{bmatrix}2\alpha f'q'+2\alpha\xi p'q'+(2\alpha\eta+1)f'q''+(2\alpha\eta+1)\xi p'q''-8\alpha p\theta''-(2\alpha\eta+1)p\theta'''\\-4\alpha fq''-(2\alpha\eta+1)fq'''-4\alpha\xi pq''-(2\alpha\eta+1)pf'''-(2\alpha\eta+1)\xi pp'''\end{bmatrix}\tag{41}$$

6. Discussion

Fluid flow, temperature, and entropy rate for sundry parameters regarding nanoliquid (MoS_4/engine oil) and hybrid nanoliquid (MoS_4 + $CoFe_2O_4$/engine oil) are presented. In these graphs, the solid lines denote the nanoliquid impact, and the dashed lines represent hybrid nanoliquid behavior. The numerical results for coefficient of skin friction (C_{fx}) and the thermal transport rate (Nu_x) for nanoliquid (MoS_4/engine oil) and hybrid nanoliquid (MoS_4 + $CoFe_2O_4$/engine oil) were examined.

6.1. Velocity

Fig. 2 shows the variation in the curvature variable for liquid flow. A larger approximation of curvature (α) variable leads to a decreased radius of curvature, which shrinks the region of the cylinder in contact with liquid. Consequently, resistance decreases, which hence boosts fluid flow. Fig. 3 indicates the impact of Forchheimer number on velocity. An augmentation in the Forchheimer number corresponds to a decrease in the liquid flow for nanoliquid (MoS_4/engine oil) and hybrid nanoliquid (MoS_4 + $CoFe_2O_4$/engine oil). Fig. 4 depicts the influence of the magnetic effect on liquid flow ($f'(\eta)$). A physically higher magnetic field leads to resistance to liquid flow, and as a result, velocity decreases. Fig. 5 exhibits the outcomes of the porosity variable for velocity ($f'(\eta)$). The flow was enhanced by a higher approximation of the porosity parameter.

6.2. Temperature

Fig. 6 indicates the temperature variation for thermal relaxation time parameter (β_{t}). An increase in the thermal field occurs *versus* the higher thermal relaxation time (β_{t}) parameter. The behavior of ($\theta(\eta)$) *versus* a higher radiation variable is shown in Fig. 7. Physically higher radiation leads to an additional energy

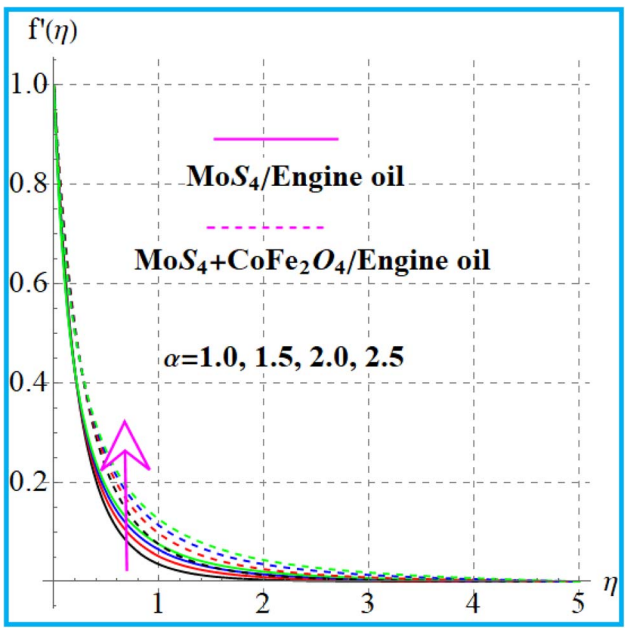

Fig. 2 $f'(\eta)$ variation *versus* α.

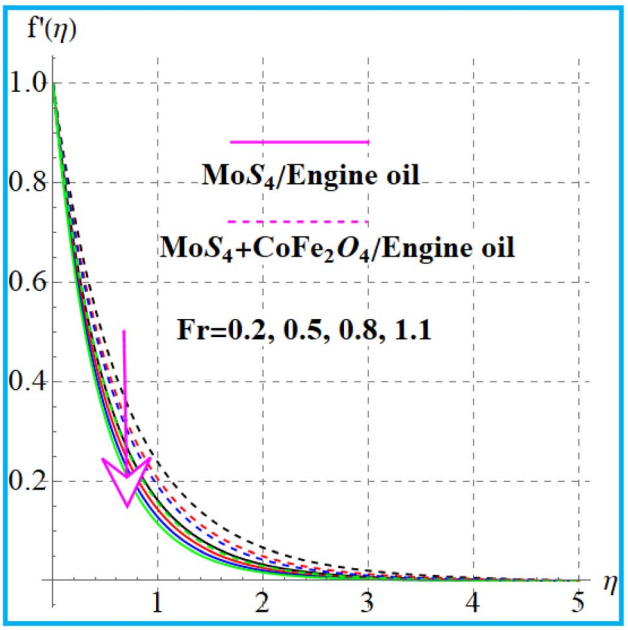

Fig. 3 $f'(\eta)$ variation *versus* Fr.

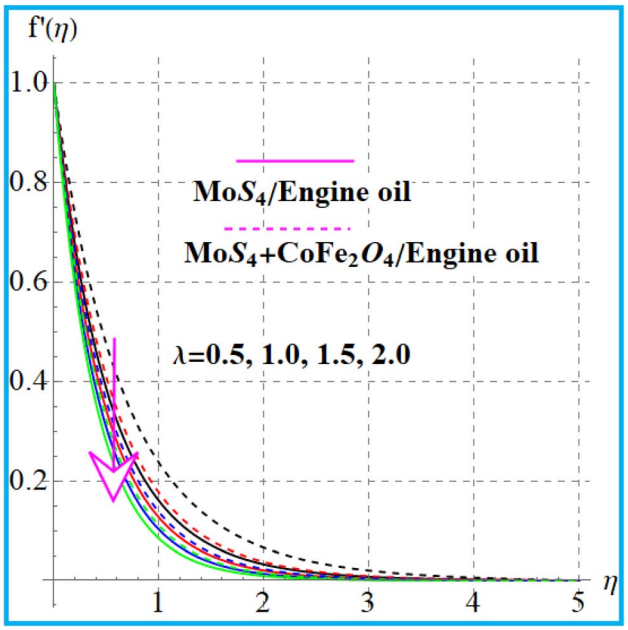

Fig. 5 $f'(\eta)$ variation *versus* λ.

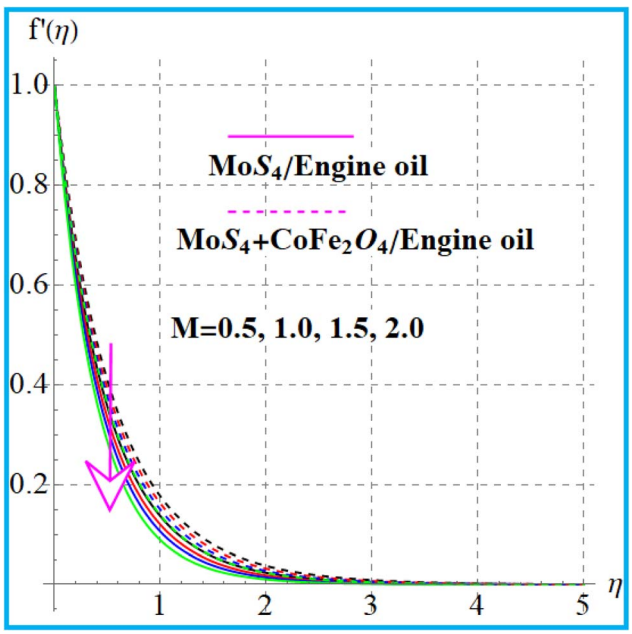

Fig. 4 $f'(\eta)$ variation *versus* M.

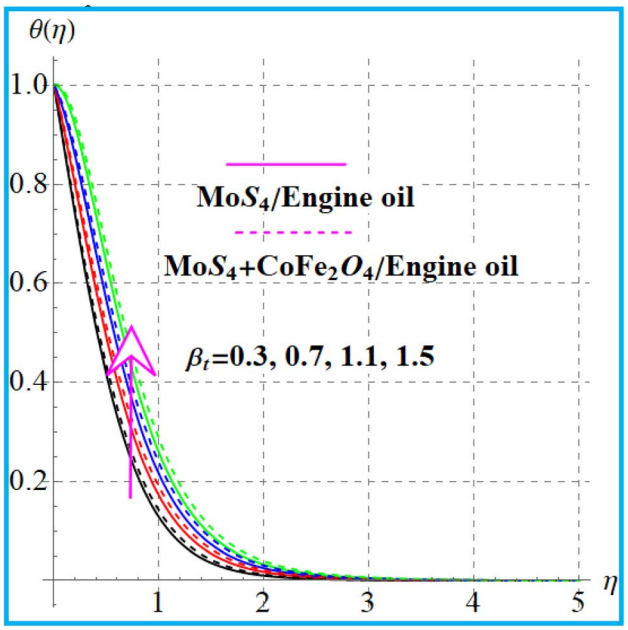

Fig. 6 $\theta(\eta)$ variation *versus* β_t.

in the system, which increases the thermal field. Fig. 8 displays outcomes of the curvature (α) variable for temperature. Temperature enhances *versus* a higher curvature parameter. Fig. 9 shows the Prandtl (Pr) number impact for ($\theta(\eta)$). Physically, (Pr) decreases the thermal diffusivity, and therefore, the temperature decreases. Fig. 10 illustrates the outcomes of heat generation for a thermal field. An increase in temperature against heat generation is possible.

6.3. Entropy rate

Fig. 11 depicts the behavior of entropy against a higher magnetic field. A physically higher magnetic force leads to an increasing resistive force, which gives rise to greater energy in the system, and thus, the entropy rate increases. Fig. 12 shows the variation of the porosity (λ) variable against the entropy rate. An increase in the entropy production occurs against a larger approximation of the porosity parameter. Fig. 13 displays the

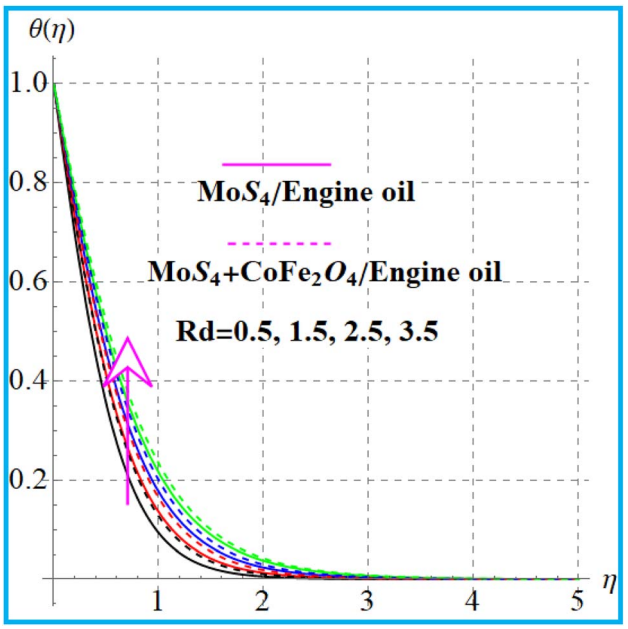

Fig. 7 $\theta(\eta)$ variation *versus* Rd.

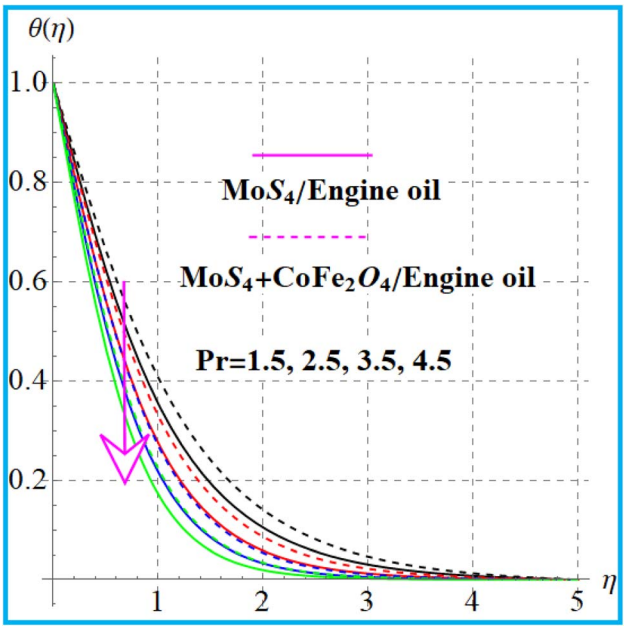

Fig. 9 $\theta(\eta)$ variation *versus* Pr.

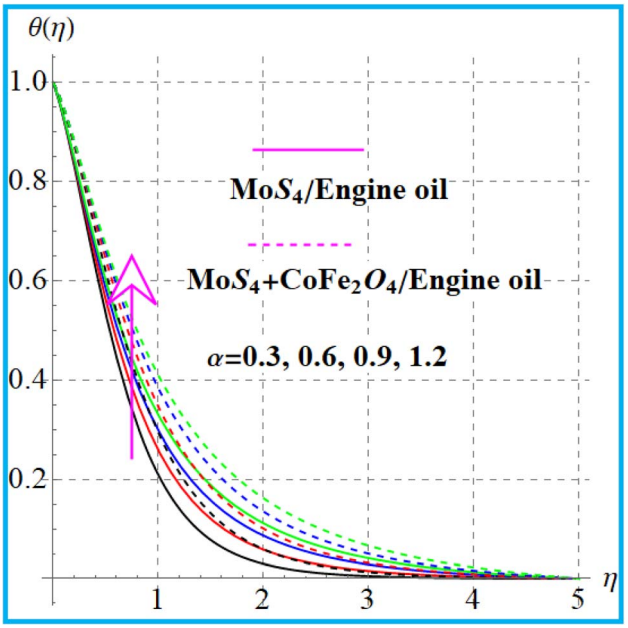

Fig. 8 $\theta(\eta)$ variation *versus* α.

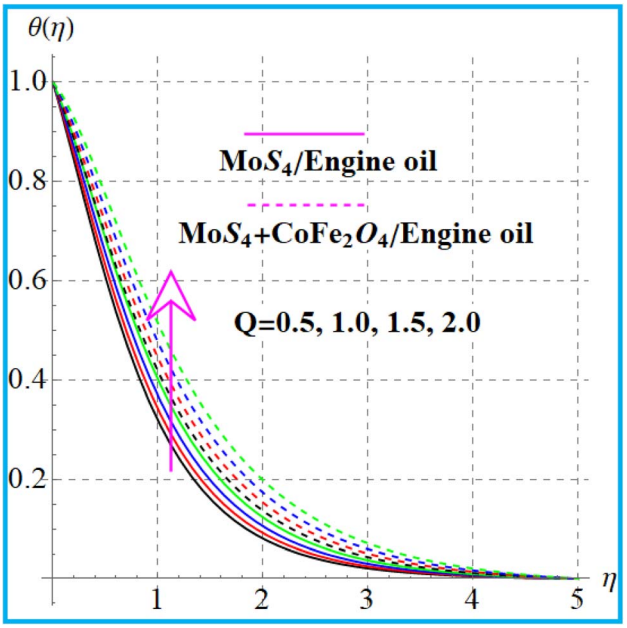

Fig. 10 $\theta(\eta)$ variation *versus* Q.

radiation variation for the entropy rate. Physically higher radiation leads to increasing thermal emission, which creates extra energy in a thermal system. As a consequence, the entropy rate increases. Fig. 14 elucidates the impact of curvature on the entropy rate. The entropy production is enhanced for the curvature variable.

6.4. Physical quantities

The numerical results for coefficient of skin friction $\left(\frac{1}{2}C_{\mathrm{fx}}\mathrm{Re}_x^{1/2}\right)$ and thermal transport rate $(\mathrm{Nu}_x\mathrm{Re}_x^{-1/2})$ for nanoliquid (MoS_4/engine oil) and hybrid nanoliquid (MoS_4 + $CoFe_2O_4$/engine oil) have been sketched in Tables 2 and 3.

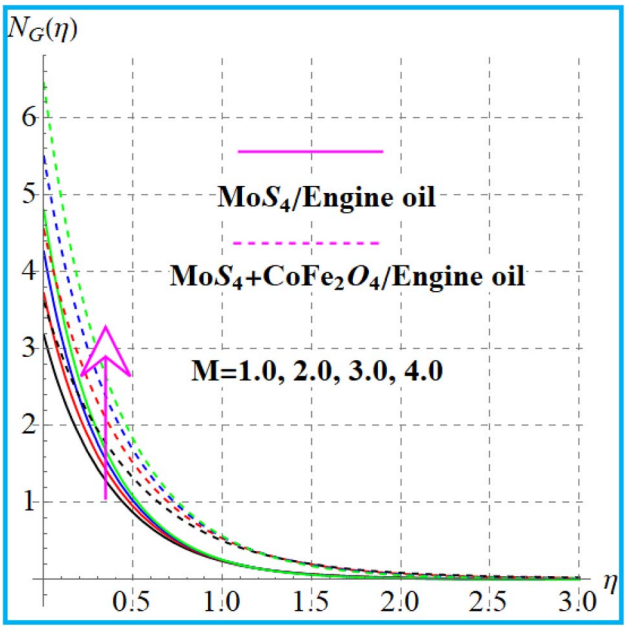

Fig. 11 $N_G(\eta)$ variation *versus* M.

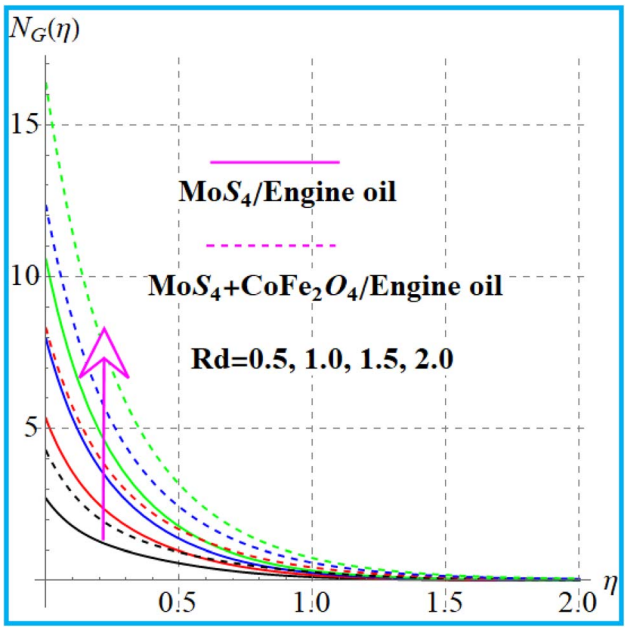

Fig. 13 $N_G(\eta)$ variation *versus* Rd.

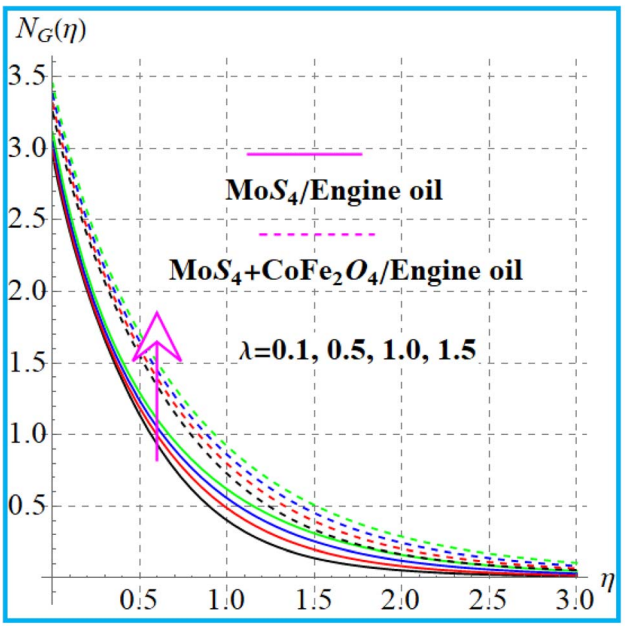

Fig. 12 $N_G(\eta)$ variation *versus* λ.

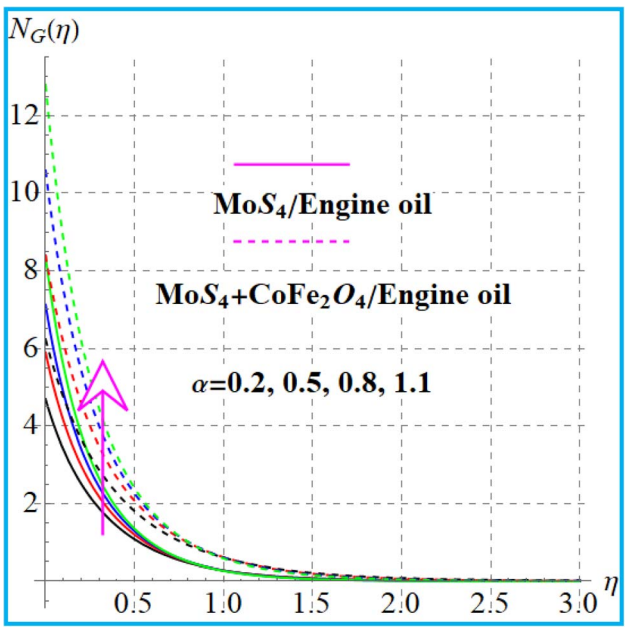

Fig. 14 $N_G(\eta)$ variation *versus* α.

6.4.1. Coefficient of skin friction. Surface drag force $\left(\frac{1}{2}C_{fx}\mathrm{Re}_x^{1/2}\right)$ for influential variables is examined in Table 2. Higher magnetic variables lead to intensification of the skin friction coefficient for nanomaterial (MoS_4/engine oil) and hybrid nanomaterial (MoS_4 + $CoFe_2O_4$/engine oil). Clearly, for a larger porosity variable and Forchheimer number, the surface drag force improved.

6.4.2. Nusselt number. Physical features of emerging variables of the Nusselt number ($Nu_x\mathrm{Re}_x^{-1/2}$) were constructed in Table 3. An increase in the heat transport rate ($Nu_x\mathrm{Re}_x^{-1/2}$) occurs through radiation and thermal relaxation time parameters. Higher estimation of heat generation variables intensifies the heat transport rate ($Nu_x\mathrm{Re}_x^{-1/2}$) for nanoliquid (MoS_4/engine oil) and hybrid nanoliquid (MoS_4 + $CoFe_2O_4$/engine oil).

Table 2 Numerical values of surface drag force $\left(\frac{1}{2}C_{fx}Re_x^{1/2}\right)$

$\frac{1}{2}C_{fx}Re_x^{1/2}$				
Fr	M	λ	MoS_4/engine oil	MoS_4 + $CoFe_2O_4$/engine oil
0.2	0.5	0.3	1.23154	1.65829
0.6			2.32562	3.09652
1.0			3.09845	3.95624
0.5	1.0	0.3	2.56234	3.56329
	2.0		3.69532	4.032654
	3.0		4.65892	5.01985
0.2	0.5	0.5	0.96523	1.85746
		1.0	1.75632	2.89635
		1.5	2.65295	3.56982

Table 3 Thermal transport rate ($Nu_xRe_x^{-1/2}$) variation against emerging parameters

$Nu_xRe_x^{-1/2}$				
Rd	β_t	Q	MoS_4/engine oil	MoS_4 + $CoFe_2O_4$/engine oil
1.5	0.5	1.0	3.42352	3.89653
2.0			4.12956	5.03256
2.5			5.45638	6.36524
1.0	1.0	1.0	2.86593	3.78654
	1.5		3.58647	4.25369
	2.0		4.96583	5.65389
1.0	0.5	1.5	2.54892	3.96585
		2.5	3.95862	4.65895
		3.5	4.96852	5.87562

7. Concluding remarks

The main results are listed below.

- The fluid flow variation for porosity and curvature variables is reversed.
- The velocity field decayed for a magnetic field, while the opposite holds for the entropy rate and temperature.
- The Forchheimer number results in velocity decrease.
- The curvature parameter variation for entropy and temperature for nanoliquid (MoS_4/engine oil) and hybrid nanoliquid (MoS_4 + $CoFe_2O_4$/engine oil) was the same.
- An enhancement of the temperature and entropy rate against radiation was observed.
- The thermal field decays for a higher Prandtl number in nanoliquid (MoS_4/engine oil) and hybrid nanoliquid (MoS_4 + $CoFe_2O_4$/engine oil).
- A higher thermal relaxation time enhances the temperature in nanoliquid (MoS_4/engine oil) and hybrid nanoliquid (MoS_4 + $CoFe_2O_4$/engine oil).
- Porosity parameter variation increases the entropy rate for nanoliquid (MoS_4/engine oil) and hybrid nanoliquid (MoS_4 + $CoFe_2O_4$/engine oil).
- A higher magnetic field intensifies the surface drag force for nanoliquid (MoS_4/engine oil) and hybrid nanoliquid (MoS_4 + $CoFe_2O_4$/engine oil).
- A larger estimation of the Forchheimer number and porosity variable leads to coefficient of skin friction enhancement for nanomaterial (MoS_4/engine oil) and hybrid nanomaterial (MoS_4 + $CoFe_2O_4$/engine oil).
- A higher radiation variable results in thermal transport rate enhancement for nanoliquid (MoS_4/engine oil) and hybrid nanoliquid (MoS_4 + $CoFe_2O_4$/engine oil).
- A higher thermal relaxation time variable improves the heat transport rate for nanoliquid (MoS_4/engine oil) and hybrid nanoliquid (MoS_4 + $CoFe_2O_4$/engine oil).
- The Nusselt number intensifies for higher heat generation.
- The skin friction coefficient for hybrid nanomaterial (MoS_4 + $CoFe_2O_4$/engine oil) was more than that of nanoliquid (MoS_4/engine oil).
- The thermal transport rate was more dominant for hybrid nanoliquid (MoS_4 + $CoFe_2O_4$/engine oil) than for nanoliquid (MoS_4/engine oil).

Conflicts of interest

There are no conflicts to declare.

References

1 S. U. S. Choi, *Enhancing thermal conductivity of fluids with nanoparticles*, ASME Publications-Fed, 1995, vol. 231, pp. 99–106.
2 J. A. Eastman, S. U. S. Choi, S. Li, W. Yu and L. J. Thompson, Anomalously increased effective thermal conductivities of ethylene glycol-based nanofluids containing copper nanoparticles, *Appl. Phys. Lett.*, 2001, **78**, 718–720.
3 M. J. P. Gallego, L. Lugo, J. L. Legido and M. M. Piñeiro, Enhancement of thermal conductivity and volumetric behavior of Fe_xO_y nanofluids, *J. Appl. Phys.*, 2011, **110**, DOI: 10.1063/1.3603012.
4 R. Nasrin, S. Parvin and M. A. Alim, Effect of Prandtl number on free convection in a solar collector filled with nanofluid, *Procedia Eng.*, 2013, **56**, 54–62.
5 S. Sivasankaran, T. Chandrapushpam, M. Bhuvaneswari, S. Karthikeyan and A. K. Alzahrani, Effect of chemical reaction on double diffusive MHD squeezing copper water nanofluid flow between parallel plates, *J. Mol. Liq.*, 2022, **368**, DOI: 10.1016/j.molliq.2022.120768.
6 M. Hussain, U. Farooq and M. Sheremet, Nonsimilar convective thermal transport analysis of EMHD stagnation Casson nanofluid flow subjected to particle shape factor and thermal radiations, *Int. Commun. Heat Mass Transfer*, 2022, **137**, DOI: 10.1016/j.icheatmasstransfer.2022.106230.
7 P. M. Patil and H. F. Shankar, Heat transfer attributes of Al_2O_3-Fe_3O_4/H_2O hybrid nanofluid flow over a yawed cylinder, *Propuls. Power Res.*, 2022, **11**, 416–429.
8 O. Çiçek, M. A. Sheremet and A. C. Baytaş, Effect of natural convection hybrid nanofluid flow on the migration and deposition of MWCNTFe3O4 in a square enclosure, *Int. J. Therm. Sci.*, 2023, **190**, DOI: 10.1016/j.ijthermalsci.2023.108318.

9 S. A. Khan, T. Hayat and A. Alsaedi, Thermal conductivity performance for ternary hybrid nanomaterial subject to entropy generation, *Energy Rep.*, 2022, **8**, 9997–10005.
10 M. Hussain and M. Sheremet, Convection analysis of the radiative nanofluid flow through porous media over a stretching surface with inclined magnetic field, *Int. Commun. Heat Mass Transfer*, 2023, **140**, DOI: 10.1016/j.icheatmasstransfer.2022.106559.
11 S. A. Abdollahi, A. Alizadeh, I. C. Esfahani, M. Zarinfar and P. Pasha, Investigating heat transfer and fluid flow betwixt parallel surfaces under the influence of hybrid nanofluid suction and injection with numerical analytical technique, *Alex. Eng. J.*, 2023, **70**, 423–439.
12 M. Shanmugapriya, R. Sundareswaran, P. S. Kumar and G. Rangasamy, Impact of nanoparticle shape in enhancing heat transfer of magnetized ternary hybrid nanofluid, *Sustain. Energy Technol. Assess.*, 2022, **53**, DOI: 10.1016/j.seta.2022.102700.
13 M. Arif, P. Kumam, W. Kumam and Z. Mostafa, Heat transfer analysis of radiator using different shaped nanoparticles water-based ternary hybrid nanofluid with applications: A fractional model, *Case Stud. Therm. Eng.*, 2022, **31**, DOI: 10.1016/j.csite.2022.101837.
14 S. Jana, A. S. Khojin and W. H. Zhong, Enhancement of fluid thermal conductivity by the addition of single and hybrid nano-additives, *Thermochimica*, 2007, **462**, 45–55.
15 M. M. Bhatti, R. Ellahi and M. H. Doranehgard, Numerical study on the hybrid nanofluid (Co_3O_4-Go/H_2O) flow over a circular elastic surface with non-Darcy medium: Application in solar energy, *J. Mol. Liq.*, 2022, **361**, DOI: 10.1016/j.molliq.2022.119655.
16 N. S. Wahid, N. M. Arifin, N. S. Khashi'ie, I. Pop, N. Bachok and M. E. H. Hafidzuddin, Hybrid nanofluid stagnation point flow past a slip shrinking Riga plate, *Chin. J. Phys.*, 2022, **78**, 180–193.
17 M. R. Zangooee, K. Hosseinzadeh and D. D. Ganji, Hydrothermal analysis of hybrid nanofluid flow on a vertical plate by considering slip condition, *Theor. App. Mech. Lett.*, 2022, **12**, DOI: 10.1016/j.taml.2022.100357.
18 S. A. Khan, T. Hayat and A. Alsaedi, Entropy optimization for nanofluid flow with radiation subject to a porous medium, *J. Pet. Sci. Eng.*, 2022, **217**, DOI: 10.1016/j.petrol.2022.110864.
19 N. A. Zainal, I. Waini, N. S. Khashi'ie, A. R. M. Kasim, K. Naganthran, R. Nazar and I. Pop, Stagnation point hybrid nanofluid flow past a stretching/shrinking sheet driven by Arrhenius kinetics and radiation effect, *Alex. Eng. J.*, 2023, **68**, 29–38.
20 S. R. R. Reddy, C. S. K. Raju, S. R. Gunakala, H. T. Basha and S. J. Yook, Bio-magnetic pulsatile CuO-Fe_3O_4 hybrid nanofluid flow in a vertical irregular channel in a suspension of body acceleration, *Int. Commun. Heat Mass Transfer*, 2022, **135**, DOI: 10.1016/j.icheatmasstransfer.2022.106151.
21 M. I. Khan, S. A. Khan, T. Hayat, M. Waqas and A. Alsaedi, Modeling and numerical simulation for flow of hybrid nanofluid (SiO_2/$C_3H_8O_2$) and (MoS_2/$C_3H_8O_2$) with entropy optimization and variable viscosity, *Int. J. Numer. Methods Heat Fluid Flow*, 2020, **22**, 3939–3955.
22 A. Z. Ullah, X. Guo, T. Gul, I. Ali, A. Saeed and A. M. Galal, Thin film flow of the ternary hybrid nanofluid over a rotating disk under the influence of magnetic field due to nonlinear convection, *J. Magn. Magn. Mater.*, 2023, **573**, DOI: 10.1016/j.jmmm.2023.170673.
23 X. Wang, Q. Wen, J. Yang, S. Shittu, X. Wang, X. Zhao and Z. Wang, Heat transfer and flow characteristic of a flat confined loop thermosyphon with ternary hybrid nanofluids for electronic devices cooling, *Appl. Therm. Eng.*, 2023, **221**, DOI: 10.1016/j.applthermaleng.2022.119758.
24 M. Yasir, M. Khan, A. S. Alqahtani and M. Y. Malik, Mass transpiration effect on rotating flow of radiative hybrid nanofluid due to shrinking surface with irregular heat source/sink, *Case Stud. Therm. Eng.*, 2023, **44**, DOI: 10.1016/j.csite.2023.102870.
25 A. S. Alnahdi, S. Nasir and T. Gul, Couple stress ternary hybrid nanofluid flow in a contraction channel by means of drug delivery function, *Math. Comput. Simul.*, 2023, **210**, 103–119.
26 X. Jiang, M. Hatami, A. Abderrahmane, O. Younis, B. M. Makhdoum and K. Guedri, Mixed convection heat transfer and entropy generation of MHD hybrid nanofluid in a cubic porous cavity with wavy wall and rotating cylinders, *Appl. Therm. Eng.*, 2023, **226**, DOI: 10.1016/j.applthermaleng.2023.120302.
27 J. Shelton, N. K. Saini and S. M. Hasan, Experimental study of the rheological behavior of TiO_2-Al_2O_3/mineral oil hybrid nanofluids, *J. Mol. Liq.*, 2023, **380**, DOI: 10.1016/j.molliq.2023.121688.
28 K. N. Sneha, G. Bognar, U. S. Mahabaleshwar, D. K. Singh and O. P. Singh, Magnetohydrodynamics effect of Marangoni nano boundary layer flow and heat transfer with CNT and radiation, *J. Magn. Magn. Mater.*, 2023, **575**, DOI: 10.1016/j.jmmm.2023.170721.
29 K. Mausam, A. Pare, S. K. Ghosh and A. K. Tiwari, Thermal performance analysis of hybrid-nanofluid based flat plate collector using Grey relational analysis (GRA): An approach for sustainable energy harvesting, *Therm. Sci. Eng. Prog.*, 2023, **37**, DOI: 10.1016/j.tsep.2022.101609.
30 R. Vinoth, B. Sachuthananthan, A. Vadivel, S. Balakrishnan and A. G. S. Raj, Heat transfer enhancement in oblique finned curved microchannel using hybrid nanofluid, *Int. J. Therm. Sci.*, 2023, **183**, DOI: 10.1016/j.ijthermalsci.2022.107848.
31 A. Bejan, A study of entropy generation in fundamental convective heat transfer, *J. Heat Transfer*, 1979, **101**, 718–725.
32 A. Bejan, Entropy generation through heat and fluid flow, *J. Appl. Mech.*, 1983, **50**, DOI: 10.1115/1.3167072.
33 M. I. Khan, S. A. Khan, T. Hayat, M. I. Khan and A. Alsaedi, Entropy optimization analysis in MHD nanomaterials (TiO_2-GO) flow with homogeneous and heterogeneous reactions, *Comput. Methods Programs Biomed.*, 2020, **184**, DOI: 10.1016/j.cmpb.2019.105111.

34 C. Kumawat, B. K. Sharma, Q. M. A. Mdallal and M. R. Gorji, Entropy generation for MHD two phase blood flow through a curved permeable artery having variable viscosity with heat and mass transfer, *Int. Commun. Heat Mass Transfer*, 2022, **133**, DOI: 10.1016/j.icheatmasstransfer.2022.105954.

35 G. P. Ashwinkumar, S. P. Samrat and N. Sandeep, Convective heat transfer in MHD hybrid nanofluid flow over two different geometries, *Int. Commun. Heat Mass Transfer*, 2021, **127**, DOI: 10.1016/j.icheatmasstransfer.2021.105563.

36 D. Rajkumar, A. S. Reddy, P. V. S. Narayana, K. Jagadeshkumar and A. J. Chamkha, Pulsating magnetohydrodynamic flow of Fe_3O_4-blood based micropolar nanofluid between two vertical porous walls with Cattaneo–Christov heat flux and entropy generation, *J. Magn. Magn. Mater.*, 2023, **571**, DOI: 10.1016/j.jmmm.2023.170564.

37 U. M. Zahid, Y. Akbar and F. M. Abbasi, Entropy generation analysis for peristaltically driven flow of hybrid nanofluid, *Chin. J. Phys.*, 2020, **67**, 330–348.

38 A. Mahesh, S. V. K. Varma, C. S. K. Raju, M. J. Babu, K. Vajravelu and W. Al-Kouz, Significance of non-Fourier heat flux and radiation on PEG – Water based hybrid Nanofluid flow among revolving disks with chemical reaction and entropy generation optimization, *Int. Commun. Heat Mass Transfer*, 2021, **127**, DOI: 10.1016/j.icheatmasstransfer.2021.105572.

39 J. Chen, R. Zhao, Y. L. Nian and W. L. Cheng, Numerical study on the effects of cylindrical roughness on heat transfer performance and entropy generation of supercritical carbon dioxide in vertical tubes, *Int. J. Heat Mass Transfer*, 2023, **208**, DOI: 10.1016/j.ijheatmasstransfer.2023.124060.

40 L. S. Sundar and H. K. Mewada, Experimental entropy generation, exergy efficiency and thermal performance factor of $CoFe_2O_4$/Water nanofluids in a tube predicted with ANFIS and MLP models, *Int. J. Therm. Sci.*, 2023, **190**, DOI: 10.1016/j.ijthermalsci.2023.108328.

41 S. A. Khan, T. Hayat, A. Alsaedi and B. Ahmad, Melting heat transportation in radiative flow of nanomaterials with irreversibility analysis, *Renewable Sustainable Energy Rev.*, 2021, **140**, DOI: 10.1016/j.rser.2021.110739.

42 P. S. Salimath and I. S. Ertesvåg, Local entropy generation and entropy fluxes of a transient flame during head-on quenching towards solid and hydrogen-permeable porous walls, *Int. J. Hydrogen Energy*, 2021, **46**, 26616–26630.

43 L. S. Sundar, S. Mesfin, E. V. Ramana, Z. Said and A. C. M. Sousa, Experimental investigation of thermo-physical properties, heat transfer, pumping power, entropy generation, and exergy efficiency of nanodiamond + Fe_3O_4/60:40% water-ethylene glycol hybrid nanofluid flow in a tube, *Therm. Sci. Eng. Prog.*, 2021, **21**, DOI: 10.1016/j.tsep.2020.100799.

44 P. Barnoon, D. Toghraie, F. Eslami and B. Mehmandoust, Entropy generation analysis of different nanofluid flows in the space between two concentric horizontal pipes in the presence of magnetic field: Single-phase and two-phase approaches, *Comput. Math. Appl.*, 2019, **77**, 662–692.

45 S. Das, N. Mahato, A. Ali and R. N. Jana, Dynamical behaviour of magneto-copper-titania/water-ethylene glycol stream inside a gyrating channel, *Chem. Phys. Lett.*, 2022, **793**, DOI: 10.1016/j.cplett.2022.139476.

46 Z. Mahmood, U. Khan, S. Saleem, K. Rafique and S. M. Eldin, Numerical analysis of ternary hybrid nanofluid flow over a stagnation region of stretching/shrinking curved surface with suction and Lorentz force, *J. Magn. Magn. Mater.*, 2023, **573**, DOI: 10.1016/j.jmmm.2023.170654.

47 N. A. Zainal, I. Waini, N. S. Khashi'ie, A. R. M. Kasim, K. Naganthran, R. Nazar and I. Pop, Stagnation point hybrid nanofluid flow past a stretching/shrinking sheet driven by Arrhenius kinetics and radiation effect, *Alex. Eng. J.*, 2023, **68**, 29–38.

48 B. Saleh and L. S. Sundar, Entropy generation and exergy efficiency analysis of ethylene glycol-water based nanodiamond + Fe_3O_4 hybrid nanofluids in a circular tube, *Powder Technol.*, 2021, **380**, 430–442.

49 A. Alsaedi, K. Muhammad and T. Hayat, Numerical study of MHD hybrid nanofluid flow between two coaxial cylinders, *Alex. Eng. J.*, 2022, **61**, 8355–8362.

50 I. Waini, U. Khan, A. Zaib, A. Ishak and I. Pop, Inspection of TiO_2-$CoFe_2O_4$ nanoparticles on MHD flow toward a shrinking cylinder with radiative heat transfer, *J. Mol. Liq.*, 2022, **361**, DOI: 10.1016/j.molliq.2022.119615.

51 M. A. Qureshi, A case study of MHD driven Prandtl-Eyring hybrid nanofluid flow over a stretching sheet with thermal jump conditions, *Case Stud. Therm. Eng.*, 2021, **28**, DOI: 10.1016/j.csite.2021.101581.

52 H. Waqas, S. M. R. S. Naqvi, M. S. Alqarni and T. Muhammad, Thermal transport in magnetized flow of hybrid nanofluids over a vertical stretching cylinder, *Case Stud. Therm. Eng.*, 2021, **27**, DOI: 10.1016/j.csite.2021.101219.

53 H. Waqas, M. Fida, D. Liu, U. Manzoor and T. Muhammad, Numerical simulation of entropy generation for nanofluid with the consequences of thermal radiation and Cattaneo–Christov heat flux model, *Int. Commun. Heat Mass Transfer*, 2022, **137**, DOI: 10.1016/j.icheatmasstransfer.2022.106293.